American Mineralogist, Volume 94, pages 676–683, 2009

The crystal chemical role of Zn in alunite-type minerals: Structure refinements for kintoreite and zincian kintoreite

Ian E. Grey,[1,*] W. Gus Mumme,[1] Stuart J. Mills,[2] William D. Birch,[3] and Nicholas C. Wilson[1]

[1]CSIRO Minerals, Box 312, Clayton South, Victoria 3169, Australia
[2]University of British Columbia, Department of Earth and Ocean Sciences, Vancouver, British Columbia V6T 1Z4, Canada
[3]Geosciences, Museum Victoria, GPO Box 666, Melbourne, Victoria 3001, Australia

Abstract

Kintoreite, $PbFe_3H_{0.94}[(PO_4)_{0.97}(SO_4)_{0.03}]_2(OH)_6$, and zincian kintoreite, $PbZn_{0.3}Fe_3H_{0.24}[(PO_4)_{0.54}(SO_4)_{0.08}(AsO_4)_{0.38}]_2(OH)_6$, have rhombohedral symmetry, space group $R\bar{3}m$, with hexagonal cell parameters $a = 7.2963(5)$ Å, $c = 16.8491(5)$ Å, and $a = 7.3789(3)$ Å, $c = 16.8552(7)$ Å, respectively. The structures have been refined using single-crystal X-ray data to $R_1 = 0.030$ for 374 observed reflections and $R_1 = 0.035$ for 399 observed reflections, respectively. The structures of both minerals comprise rhombohedral stacking of (001) composite layers of corner-shared octahedra and tetrahedra with Pb atoms occupying icosahedral sites between the layers, as in the alunite-type structure. The corner-connected octahedra form three-membered and six-membered rings as in hexagonal tungsten bronzes. The structure of zincian kintoreite differs from other alunite-type structures in having partial occupation, by Zn, of new sites within the six-membered rings in the octahedral layers. The Zn is displaced to an off-center position in the hexagonal ring, where it assumes fivefold trigonal-bipyramidal coordination, to three of the hydroxyl anions forming the ring, and to the apical O anions of the XO_4 tetrahedra on opposite sides of the ring. The different structural modes of Zn incorporation into SO_4-dominant and $(P,As)O_4$-dominant members of $A^{2+}B_3^{3+}(XO_4)_2(OH)_6$ alunite-type minerals are discussed in terms of the different charge-compensation mechanisms involved.

Keywords: Zincian kintoreite, crystal structure, alunite-type structure, single-crystal study

Introduction

Minerals of the alunite supergroup, with general composition $AB_3(XO_4)_2(OH)_6$, are remarkable for the diversity of elements that can be incorporated into the three types of cation sites: A, B, and X. The icosahedral A sites incorporate a range of large cations including monovalent Na^+, K^+, Rb^+, NH_4^+, H_3O^+, divalent Ca^{2+}, Sr^{2+}, Ba^{2+}, Pb^{2+}, and trivalent Bi^{3+}, Ln^{3+} (Ln = lanthanide) elements. The B sites are octahedrally coordinated and are usually occupied by trivalent cations, Fe^{3+}, Al^{3+}, Cr^{3+}, V^{3+}, and Ga^{3+}, but are known to also incorporate divalent Cu^{2+} and Zn^{2+}, as well as pentavalent Sb^{5+}. The X sites are tetrahedral, most commonly occupied by S^{6+}, P^{5+}, and As^{5+} but can also contain C^{4+}, Cr^{6+}, and Si^{4+} (Scott 1987; Kolitsch and Pring 2001). Extensive solid solutions involving mixed substitution at one or more of the three sites are common. The composition often requires modification to accommodate different combinations of cations. Such modifications include hydroxyl substitution for oxygen in the XO_4 tetrahedra, substitution of H_2O or oxygen for OH, and partial occupancy of the A and/or B sites (Jambor 1999).

The majority of alunite-type minerals have rhombohedral symmetry, space group $R\bar{3}m$, with hexagonal cell parameters $a \sim 7$ Å, $c \sim 17$ Å (Jambor 1999). The structure is made up of (001) sheets of corner-shared octahedra and tetrahedra, which are stacked along c according to the rhombohedral symmetry. The A atoms occupy icosahedral sites between the layers. The stacking of two composite octahedral/tetrahedral layers, with interlayer A atoms, is shown in Figure 1. The octahedra share corners via hydroxyl anions, labeled O3 in Figure 1, to form a planar network of triangular clusters, encompassing hexagonal voids. Such a motif is common to many structures including those of zirconolite polytypes, pyrochlore, and hexagonal tungsten bronze (HTB) phases, and is often described as a HTB layer (e.g., Grey et al. 2006). The apical oxygen anions (O2 in Fig. 1) of the triangular groupings of octahedra are shared with the XO_4 tetrahedra. The corner-shared octahedra in the HTB layer have considerable flexibility to tilt about the corner-linkages to accommodate different sized XO_4 tetrahedra. This is a major contributing factor to the compositional diversity of the alunite-type minerals.

The three different cation sites in the alunite-type minerals have quite different sizes and valency requirements, and so generally there is no ambiguity in assigning cations to the A, B, or X sites. Possible exceptions include Cr, that can occupy the B site as Cr^{3+} and the X site as Cr^{6+}, and elements such as Ge^{4+}, that readily adopt both tetrahedral and octahedral coordination (Mills et al. 2006).

* E-mail: ian.grey@csiro.au

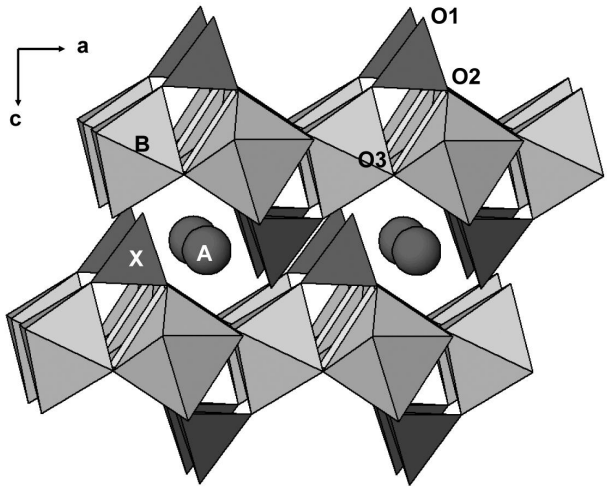

FIGURE 1. Polyhedral representation of the stacking of two composite layers of octahedra and tetrahedra in the alunite-type structure. The ideal A atom positions are represented by the filled circles.

Another interesting case is divalent zinc. In alunite and jarosite minerals, where $XO_4 = SO_4$ and B = dominant Al or Fe, respectively, Zn substitutes for Fe/Al in the B site. Jambor and Dutrizac (1983) report up to 0.34 atoms of Zn substituting for Fe per formula unit (pfu) in synthetic plumbojarosite, while Scott (1987) reports up to 0.62 atoms of Zn substituting for Al pfu in natural alunite minerals. Zinc is reported to follow Cu in substituting at the B site in beaverite, $Pb(Fe,Cu,Zn)_3(SO_4)_2(OH)_6$, (Jambor and Dutrizac 1983; Sato et al. 2008) and in osarizawaite, $Pb(Al,Cu,Zn)_3(SO_4)_2(OH)_6$ (Giuseppetti and Tadini 1980).

In contrast to Zn occupying the B site in the alunite-type minerals, we have recently found different behavior for Zn in the zincian arsenate mineral, $PbZn_{0.5}Fe_3(AsO_4)_2(OH)_6$ (Grey et al. 2008). This mineral has a composition very similar to that of segnitite, $PbFe_3H(AsO_4)_2(OH)_6$ (Birch et al. 1992). The Zn atom occupies a new site, previously unreported for alunite-type minerals, within the hexagonal rings of the HTB layers. The Zn is displaced to an off-center position in the hexagonal ring, where it takes up fivefold trigonal bipyramidal coordination, to three of the hydroxyl anions forming the ring, and to the apical O anions of the AsO_4 tetrahedra on opposite sides of the ring. This meets the valence requirement of the apical X-O oxygen, which is otherwise severely undersaturated when X is a pentavalent cation like As^{5+}. $PbZn_{0.5}Fe_3(AsO_4)_2(OH)_6$ has a monoclinic superstructure of the alunite-type structure due to ordering of the Zn atoms into sites in half of the available hexagonal rings.

We were interested to determine if the occupation of sites within the hexagonal rings by Zn was a more general phenomenon when the tetrahedral site was occupied predominantly by pentavalent cations, As^{5+} or P^{5+}. A search was made by one of us (W.D.B.) of analytical data collected on alunite-type samples kept in the mineral collection at Museum Victoria. The search revealed a zincian kintoreite sample (kintoreite has dominant P in the X site) containing up to almost 5 wt% ZnO. Structure refinements were conducted on a single crystal of this sample, to determine the location of the Zn. A single-crystal study was also conducted on an almost pure end-member kintoreite composition for comparison. A structure refinement has been reported previously for a Zn-free kintoreite sample containing substantial substitution of As and S for P, $PbFe_3(PO_4)_{1.3}(AsO_4)_{0.4}(SO_4)_{0.3}(OH,H_2O)_6$, by Kharisun et al. (1997). The results of the structure refinements, together with electron microprobe studies of inter-element correlations in the samples, are reported here.

EXPERIMENTAL METHODS

Samples

The zincian kintoreite and pure kintoreite samples were obtained from the Museum Victoria mineral collection, with museum identification numbers M38171 and M48997, respectively. The zincian kintoreite comes from the Kintore open cut mine at Broken Hill, New South Wales. Birch and van der Heyden (1997) have described in detail the location of various oxidized zones and mineral assemblages at the Kintore open cut. The hand specimen was taken from the 280 m RL level, in the Main Shear Zone (shown in Fig. 7 of Birch and van der Heyden 1997). The dark-greenish yellow crystals are located in cavities in heavily oxidized siliceous ore consisting of granular quartz impregnated by goethite. The amber-colored crystals of pure kintoreite are from the Schöne Aussicht mine, near Dernbach, Germany. They are associated with quartz, goethite, and pyromorphite. The original specimen is in the Smithsonian Institution, number B13907.

Electron microprobe analyses

Sectioned and polished crystals were examined in a scanning electron microscope using a back-scattered electron (BSE) detector. The crystals were analyzed using a JEOL Hyperprobe operated in wavelength dispersive mode at an accelerating voltage of 15 kV, beam current of 20 nA and a spot size of 2 µm. The low voltage used, together with the use of a light element detector, allowed the sample to be analyzed directly for oxygen. Standards used were: anglesite, $PbSO_4$, for the Pb$M\alpha$, S$K\alpha$, and O$K\alpha$ lines; $MgAl_2O_4$ for Al$K\alpha$; chalcopyrite, $CuFeS_2$, for Cu$K\alpha$; hematite, Fe_2O_3, for Fe$K\alpha$; apatite, $Ca_5(PO_4)_3OH$, for P$K\alpha$; ZnS for Zn$L\alpha$; and InAs for As$L\alpha$. The results of microprobe analyses for the two samples are reported in Table 1.

The raw electron microprobe measurements were initially corrected for ZAF (atomic number/absorption/fluorescence) matrix effects using the JEOL matrix correction software. However, calculations of formulae using the corrected data gave compositions at variance with the alunite-type formula. The deviations were greatest for high-As compositions. A change was then made to external processing of the raw data using the PAP matrix correction (Pouchou and Pichoir 1993). This gave a marked improvement in the fit of the formulae to the general alunite-type formula. The change in correction procedure adjusted the As analyses by 10–15%, with smaller changes to other elements.

The zincian kintoreite crystals are chemically zoned (Fig. 2), and separate point analyses were made within the bright and dark regions, as well as composite areas where the zoning is very fine. Average analyses for the bright and dark regions as well as for all 50 point analyses are given in Table 1. The point analyses were used in element-element scatter plots to determine inter-element correlations.

Structure refinements

Single-crystal intensity data on zincian kintoreite and pure kintoreite crystals were collected at room temperature using a Bruker APEX II Kappa CCD diffractometer. The data collection and processing conditions are summarized in Table 2. The CCD intensity data sets were processed to produce absorption-corrected data files. The structure refinements, in the rhombohedral space group $R\bar{3}m$, were conducted within the WinGX program system (Farrugia 1999), using SHELX-97 (Sheldrick 1997) for the refinements. Some refinements in lower symmetries, coupled with twinning, were conducted using JANA2000 (Petricek and Dusek 2000).

The published coordinates for Pb, Fe, P, and O in kintoreite studied by Kharisun et al. (1997) were used to initiate the refinement of the pure kintoreite data in $R\bar{3}m$. The model of Kharisun et al. (1997) has the Pb atom displaced from (0,0,0) to a general 36*i* position (–0.018, 0.038, 0.0005). We also tested models for the displacement of the Pb atom to sites 18*f* (x,0,0) and 18*h* (*x*,–*x*,*z*). Both of the latter sites gave comparable refinements with slightly lower *R* factors than for the Kharisun et al. model. We report the (*x*,0,0) position for displaced Pb, consistent with refinements for related minerals (Szymanski 1988; Kolitsch et al. 1999). In reality, both (*x*,0,0) and (*x*,–*x*,*z*; where $z \sim 0$) are equally valid approximations to the Pb distribution, which lies on an annulus in the (001) plane around the

TABLE 1. Electron microprobe analyses (wt%) for zincian kintoreite and pure kintoreite

	Zincian kintoreite					Pure kintoreite	
	Bright zones		Dark zones		All		
	Average (14)	Range	Average (24)	Range	Average (50)	Average (6)	Range
Pb	28.8	27.9–29.8	30.0	29.1–31.0	29.4	30.9	3.06–31.1
Fe	22.4	21.4–23.0	23.3	22.3–24.1	22.9	24.0	23.2–24.6
Al	0.01	0–0.04	0.02	0–0.08	0.02	0.04	0.01–0.07
Cu	0.12	0.05–0.69	0.37	0–1.31	0.28	0.28	0.21–0.50
Zn	3.06	2.30–3.82	1.48	0.38–3.73	2.22	0.22	0.16–0.25
P	4.27	3.28–6.03	5.05	2.31–7.40	4.49	8.99	8.61–9.17
S	0.25	0.14–0.40	0.98	0.10–2.53	0.66	0.28	0.13–0.59
AS	9.71	6.16–11.9	5.92	1.96–7.76	8.02	0.01	0–0.04
O	31.7	31.1–32.8	33.2	32.3–33.7	32.5	36.3	35.8–36.9
Total	100.4		100.3		100.4	100.9	

Note: Average compositions, normalized to 2[P + S + As]:
Zincian kintoreite, bright zones: $Pb_{1.01}Cu_{0.01}Zn_{0.34}Fe_{2.92}H_{0.46}(PO_4)_{1.00}(SO_4)_{0.06}(AsO_4)_{0.94}(OH)_6$;
Zincian kintoreite, dark zones: $Pb_{1.06}Cu_{0.04}Zn_{0.17}Fe_{3.06}H_{0.06}(PO_4)_{1.20}(SO_4)_{0.22}(AsO_4)_{0.58}(OH)_6$;
Zincian kintoreite, all analyses: $Pb_{1.04}Cu_{0.03}Zn_{0.24}Fe_{3.01}H_{0.19}(PO_4)_{1.06}(SO_4)_{0.16}(AsO_4)_{0.78}(OH)_6$;
Pure kintoreite: $Pb_{1.00}Cu_{0.03}Zn_{0.02}Fe_{2.87}H_{1.23}(PO_4)_{1.94}(SO_4)_{0.06}(OH)_6$.

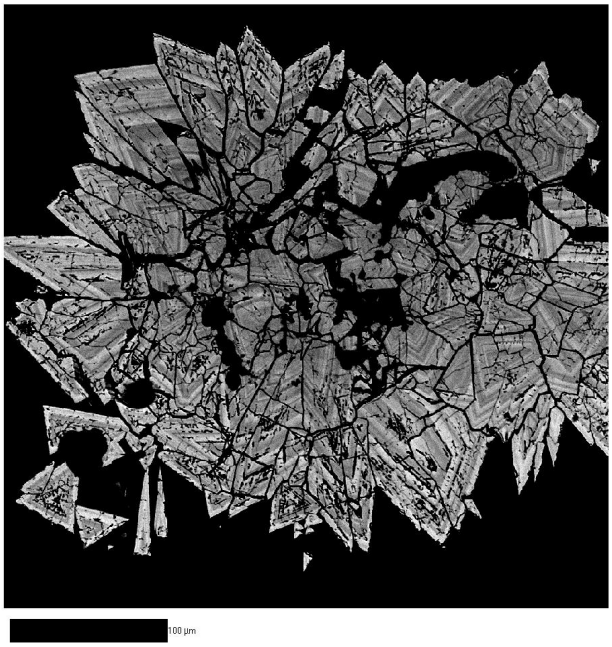

FIGURE 2. Back-scattered electron image of zincian kintoreite crystals.

origin (Kolitsch et al. 1999).

The pure kintoreite refinement converged to R_1 = 0.036 for 399 observed reflections, using anisotropic displacement parameters for all non-hydrogen atoms. A difference Fourier map showed the strongest peak at (0.18, –0.18, 0.1), located 0.9 Å from O3, which is the anion involved in corner sharing of the octahedra (Fig. 1). It is generally accepted that the O3 anion, which has a low valence sum of ~1.2, is a hydroxyl ion (Giuseppetti and Tadini 1989; Kharisun et al. 1997; Dzikowski et al. 2006). Addition of H and refinement of its coordinates and isotropic displacement parameter resulted in a small decrease in R_1 to 0.034. Further details of the refinement are given in Table 2. The refined coordinates and equivalent isotropic displacement parameters are reported in Table 3. Selected bond distances are given in Table 4.

The refinement of the zincian kintoreite data was also initiated using the coordinates of Kharisun et al. (1997). As was included with P at the X site and the proportions of each element were allowed to refine. Refinement of all coordinates and anisotropic displacement parameters converged at R_1 = 0.056 for 378 observed reflections. A difference Fourier map showed a strong peak at (0.065, –0.065, 0.495) with height of 5.1 e/Å^3. The next strongest peak had a much lower height, 0.7 e/Å^3. The strong peak was displaced by 0.83 Å from the center of the hexagonal ring in the HTB layer and was located at 1.7–1.9 Å from three anions and at 2.38 Å from two other anions. Its position and coordination correspond closely to that of the Zn atom in monoclinic $PbZn_{0.5}Fe_3(AsO_4)_2(OH)_6$ (Grey et al. 2008).

Addition of a Zn atom at (0.065, –0.065, 0.495) and refinement of its coordinates and site occupation parameter (U fixed at 0.02) improved the fit considerably, with a lowering of R_1 to 0.033 and a decrease in the goodness of fit from 2.34 to 1.16. Release of the anisotropic displacement parameters for Zn lowered R_1 further to 0.030. We were unable to unambiguously identify the location of the H atoms in a subsequent difference Fourier map, as had been possible for pure kintoreite. Further refinement details are given in Table 2. The refined coordinates and equivalent isotropic displacement parameters are reported in Table 3. Selected bond distances are given in Table 4.

In contrast to the ordering of Zn atoms into sites in half of the hexagonal rings in monoclinic $PbZn_{0.5}Fe_3(AsO_4)_2(OH)_6$ (Grey et al. 2008), the Zn atoms are randomly distributed over all such sites in the $R\bar{3}m$ structure of zincian kintoreite. We were interested to establish whether short-range ordering occurred in lower symmetry domains, which then emulate the rhombohedral symmetry by twinning. By analogy with monoclinic $PbZn_{0.5}Fe_3(AsO_4)_2(OH)_6$ ($C2/c$) and other alunite-type minerals involving cation ordering into different sites, such as gorceixite (Cm = Radoslovich 1982) and monoclinic jarosite ($C2/m$ = Gottlicher and Gasharova 1999), the most likely symmetry for such a local order is C-centered monoclinic. Application of the matrix transformation (1 –1 0/1 1 0/–1/3 1/3 1/3) to the hexagonal cell generates a C-centered monoclinic cell with a = 12.776, b = 7.381, c = 7.048 Å, β = 127.14°. Averaging of the intensity data in the monoclinic cell gave R_{int} = 0.038 for 2/m point symmetry. Of the three possible space groups consistent with the extinction conditions, $C2/m$, Cm, and $C2$, the centrosymmetric space group $C2/m$ gave the lowest figure of merit in the WinGX AssignSG routine.

The atomic coordinates were transformed to the equivalent positions in the $C2/m$ cell. Refinement in the monoclinic space group gave a splitting of Zn atom positions in the hexagonal rings similar to that obtained in the refinement of monoclinic $PbZn_{0.5}Fe_3(AsO_4)_2(OH)_6$ (Grey et al. 2008), lending support to the possibility of short-range order in the zincian kintoreite. A significant improvement to the refinement in $C2/m$ (decrease of R_1 from 0.042 to 0.031) was obtained by allowing for 120° rotational twinning about **c*** (equivalent to the hexagonal **c** direction). Refinement with anisotropic displacement parameters converged to R_1 = 0.031 for 921 observed reflections. Although this is comparable to the refinement obtained in $R\bar{3}m$, the refinement in $C2/m$ involves twice as many parameters, and so is not justified on statistical grounds. In the following discussion, we use the simpler description of the structure in $R\bar{3}m$.

RESULTS AND DISCUSSION

Electron microprobe results

A BSE image of zincian kintoreite crystals (Fig. 2) shows sharp oscillatory zoning parallel to the crystal faces. Such zoning is common in alunite-type minerals, and specifically in samples from the oxidized zone of the Broken Hill ore body (Rattray et al. 1996). The averages of microprobe analyses from the bright and dark regions are given in Table 1. The results show that the

TABLE 2. Summary of crystal data, collection, and refinement conditions for zincian kintoreite and pure kintoreite

	Zincian kintoreite	Pure kintoreite
Formula	$PbZn_{0.3}Fe_3H_{0.24}[(PO_4)_{0.54}(SO_4)_{0.08}(AsO_4)_{0.38}]_2(OH)_6$	$PbFe_3H_{0.94}[(PO_4)_{0.97}(SO_4)_{0.03}]_2(OH)_6$
Crystal data		
Space group	$R\bar{3}m$	$R\bar{3}m$
Unit-cell parameter (Å)	a = 7.3789(3), c = 16.8552(7)	a = 7.2963(5), c = 16.8491(5)
Volume (Å^3)	794.8	776.8
Z	3	3
Molecular weight	720.1	667.7
Calculated density (g/cm^3)	4.51	4.28
Crystal size (mm)	lath, 0.05 × 0.07 × 0.15	0.07 × 0.08 × 0.16
Absorption coefficient (mm^{-1})	23.2	20.7
Data collection		
Collection mode	3 × φ scans + Ω scan, 0.5° steps, 90 s per frame	2 × φ scans + 2 × Ω scans, 0.5° steps, 150 s per frame
Wavelength	Mo$K\alpha$	Mo$K\alpha$
2θ max (°)	70.0	71.1
Total no. reflections	4728	3707
No. unique reflections	461	463
No. reflections, $F > 4\sigma(F)$	374	399
Absorption correction	Multi-scan (SADABS) Tmin/Tmax = 0.52	Multi-scan (SADABS) Tmin/Tmax = 0.60
R(int)	0.046	0.055
Refinement		
No. parameters refined	37	35
R_1, $F > 4\sigma(F)$	0.030	0.035
R_1, all reflections	0.045	0.047
wR_2, all reflections	0.054	0.068
G.o.F.	1.18	1.25
Max/min residual electron density	+0.77, –0.64 e/Å^3	+1.07, –0.79 e/Å^3

TABLE 3. Refined atomic coordinates and equivalent isotropic displacement parameters (Å^2)

Atom	Site	x	y	z	U_{eq}	Occupancy
Zincian kintoreite						
Pb	18*f*	0.0630(3)	0	0	0.0313(7)	⅙
Fe	9*d*	½	0	½	0.0133(4)	1
Zn	18*h*	0.0653(7)	–0.0653(7)	0.4954(6)	0.025(2)	0.31(1)/6
X	6*c*	0	0	0.31364(5)	0.0102(2)	0.617(6) P+S +0.383(6) As
O1	6*c*	0	0	0.5937(3)	0.024(1)	1
O2	18*h*	0.2158(2)	–0.2158(2)	–0.0534(2)	0.0193(5)	1
O3	18*h*	0.1272(2)	–0.1272(2)	0.1330(2)	0.0153(4)	1
Pure kintoreite						
Pb	18*f*	0.0537(4)	0	0	0.0196(7)	⅙
Fe	9*d*	½	0	½	0.0094(1)	1
P	6*c*	0	0	0.3148(1)	0.0088(4)	1
O1	6*c*	0	0	0.5954(2)	0.0135(7)	1
O2	18*h*	0.2193(2)	–0.2193(2)	–0.0516(1)	0.0173(4)	1
O3	18*h*	0.1272(2)	–0.1272(2)	0.1324(1)	0.0093(4)	1
H1	18*h*	0.184(4)	–0.184(4)	0.100(3)	0.03(1)	1

TABLE 4. Selected bond distances (Å) for zincian kintoreite and pure kintoreite

	Zincian kintoreite		Pure kintoreite
Pb-O2	2.532(3) ×2		2.590(3) ×2
	2.938(2) ×2		2.931(2) ×2
	3.294(3) ×2		3.237(3) ×2
Pb-O3	2.563(3) ×2		2.574(3) ×2
	2.807(2) ×2		2.778(3) ×2
	3.031(3) ×2		2.968(3) ×2
Fe-O2	2.010(2) ×2		2.049(3) ×2
Fe-O3	2.010(1) ×4		1.992(1) ×4
X-O1	1.561(5)		1.512(5)
X-O2	1.606(3) ×3		1.545(2) ×3
Zn-O1	1.72(1)	O3-H1	0.90(6)
	1.86(1)		
	1.91(1)		
Zn-O3	2.383(4) ×2		

higher BSE contrast (higher average atomic number) is due to higher levels of As in the bright zones. The Zn is also higher, whereas the concentrations of the other abundant, high-atomic-number elements, Pb and Fe, are actually slightly lower in the bright zones.

A plot of atoms of As vs. atoms of (P + S) (Fig. 3a) for all analyses of zincian kintoreite shows a strong negative correlation, with R^2 = 0.975 and a slope close to –1. The analyses are relatively uniformly distributed over the full range of concentrations encountered, indicating that the bright and dark zones each encompass a range of As/(P + S) ratios as given in Table 1. The atomic fraction of As, (As)/(As + P + S), varies from 0.645 down to 0.095. This variation is the main contributor to the observed BSE image zoning.

Zinc concentrations are highest in the bright zones, associated with higher As levels. However, the correlation between Zn and As is not strong, as shown by the considerable scatter in the plot of atoms of Zn vs. atoms of As in Figure 3b. Analyses from the bright and dark zones are shown by separate symbols. High-Zn analyses group with high As values in the bright zones, but the full range of Zn analyses is represented in the dark zones. A much stronger correlation is observed for Zn vs. S (Fig. 3c). The negative correlation between atoms of Zn and atoms of S has R^2 = 0.82 based on a fit of a power law curve to the data. Levels of Zn higher than 0.1 apfu occur only for compositions containing <0.2 atoms of S pfu. At the highest S atomic concentration of 0.6 apfu, the Zn content is reduced to ~0.05 atoms Zn. There is a corresponding strong positive correlation between (Zn) and (As + P), indicating that Zn partitions into regions of the crystals where these pentavalent atoms are concentrated. Figure 3d shows that there is only a weak negative correlation between Zn and Fe atomic concentrations (R^2 = 0.6). This is in contrast to the strong negative correlation between Zn and Fe reported by Jambor and

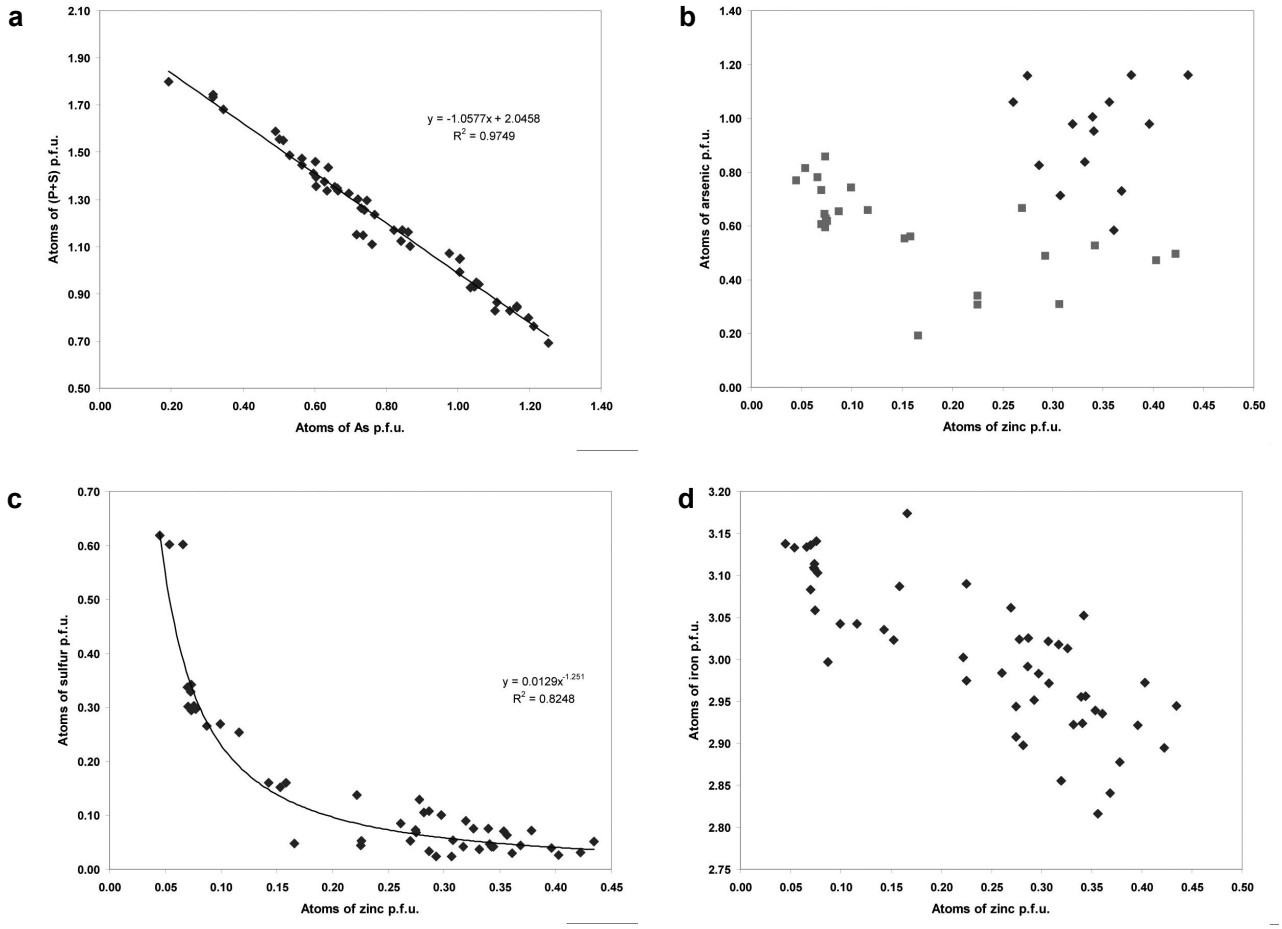

FIGURE 3. Scatter plots of microprobe analyses for zincian kintoreite. (**a**) [As] vs. [P + S], (**b**) [Zn] vs. [As]. Squares and diamonds represent analyses from dark and bright zones, respectively (analyses from zone boundaries not shown). (**c**) [Z] vs. [S]. (**d**) [Zn] vs. [Fe].

Dutrizac (1983) for synthetic jarosite compositions, where Zn substitutes for Fe in the B site.

Formulae obtained from the microprobe analyses, normalized to 2(P + S + As) as recommended by Scott (1987) are given in Table 1. Protons have been added for charge balance. The pure kintoreite sample shows a deficiency in the B site. However, this was not borne out by the single-crystal refinement of site occupancy, which was consistent with full occupancy of the B site by Fe. The deficiency in Table 1 is thus presumably due to inadequacies in the microprobe analysis due to unsuitable standards or inaccurate matrix corrections as mentioned in the experimental section. Rattray et al. (1996) have discussed the problem of obtaining reliable microprobe analyses of alunite-type minerals containing Pb. In the presentation of the formulae for the two crystals in Table 2, the $PO_4/SO_4/AsO_4$ ratios are from the microprobe analyses whereas the Zn, Fe, and Pb contents are from the structure refinements. In the case of the zincian kintoreite, the atom contents represent an average for the zoned crystal.

Crystal structures

Pure kintoreite. The crystal structure parameters from the refinement of pure kintoreite are generally similar to those obtained by Kharisun et al. (1997) for a kintoreite containing 20 at% As and 15 at% S substituting for P. Due to the As content in the latter mineral, the X-O distances are considerably longer [1.533(9) Å and 1.573(5) Å ×3] than in pure kintoreite (Table 4), and this is accompanied by an expansion of the cell parameters, relative to those for pure kintoreite, by 0.5% in *a* and 0.2% in *c*. The apical X-O1 distance is shorter than the basal X-O2 distances by 0.03 to 0.04 Å in both samples. The average X-O distance of 1.537 Å in pure kintoreite agrees with a value of 1.537 Å obtained by Baur (1981) for phosphate minerals.

The Pb atom is displaced from the ideal site at the origin in both pure kintoreite and P/As/S kintoreite. Kharisun et al. (1997) arrived at a general 36*i* position for the displaced Pb by trial and error. The position obtained, (–0.018, 0.038, 0.0005), was not refined and corresponds to a displacement of the Pb by 0.363 Å from the origin. In pure kintoreite, the refinement was optimum for Pb displaced to an 18*f* position (*x*,0,0), resulting in a larger displacement from the origin of 0.392 Å. With the Pb atom fixed at the origin the agreement factor, R_1, deteriorated markedly from 0.035 to 0.18 and very large U_{11} and U_{22} displacement parameters of 0.144(3) were obtained in the refinement. This contrasts with refinements of corkite, $PbFe_3(SO_4)(PO_4)(OH)_6$ (Giuseppetti and Tadini 1987), and plumbojarosite, $PbFe_3(SO_4)_2(OH)_6$ (Szymanski 1985), containing the smaller SO_4 group, with average X-O

distances of 1.515 and 1.475 Å, respectively. For these minerals, good refinements were obtained with the Pb undisplaced at (0,0,0) (albeit with large displacement parameters).

In the refinement of beudantite, $PbFe_3(SO_4)(AsO_4)(OH)_6$ (Giuseppetti and Tadini 1989), with an average (As,S)-O distance of 1.601 Å, an improvement in the agreement factor (0.034 to 0.018) was obtained by displacing the Pb atom to (–0.0124, 0.0323, 0.0007), corresponding to a displacement of 0.294 Å from the origin. This displacement is 0.07 to 0.1 Å smaller than in the kintoreite samples, even though the average X-O distance (and cell volume) is larger. Size effects alone thus do not explain the magnitudes of the Pb displacements. It is likely that the valence sum requirement of O2, which coordinates both to Pb and X atoms, plays a role. When $X = As^{5+}$ or P^{5+}, O2 requires a greater valence contribution from Pb than when X is S^{6+}. This can be achieved by the Pb atom being displaced toward O2.

The bond valence sum (BVS) for O3 in pure kintoreite, based on non-hydrogen contributions, is only 1.24 (using bond valence parameters of Brese and O'Keeffe 1991). The additional valence of 0.76 required for charge balance at O3 can be met by coordination to hydrogen with an O3-H distance of 1.05 Å. A proton, H1, coordinated to O3, was located in a difference Fourier map for pure kintoreite. Its position and isotropic displacement parameter were refined, and the latter remained sensible, albeit elevated, at 0.03(1) $Å^2$. The refined O3-H1 distance is 0.90(6) Å, which is within three standard deviations of the distance calculated to give a BVS of 2 at O3. Underestimates of the length of the O-H distance are commonly reported from refinements of alunite-type minerals using X-ray diffraction data (Dzikowski et al. 2006).

The protons H1 form hydrogen bonds to the apical anions, O1, of the PO_4 tetrahedra. Each O1 anion is involved as an acceptor atom in three such O3-H1···O1 bonds, at a distance of 1.96 Å. With the valence contribution from the hydrogen bonds included, the BVS at O1 is 1.48 and so O1 is still significantly undersaturated. It has often been speculated that O1 is involved as both a donor and acceptor of hydrogen bonds. Blount (1974) proposed that in crandallite, a hydroxyl group is located at half of the O1 sites, and an O1-H2···O1 hydrogen bond is formed between the proton, H2, and the O1 atoms of opposing tetrahedra on either side of the hexagonal rings. In crandallite, the O1-O1 distance is 2.99 Å, whereas the O1-O1 distance in pure kintoreite is considerably longer, at 3.21 Å. If similar hydrogen bonding occurs in kintoreite, the O1-H2 distance would be expected to be very short (Nakamoto et al. 1955) and the P-O1 distance should be correspondingly elongated (Ferraris and Ivaldi 1984). However the reverse is observed; the P-O1 distance, 1.512 Å, is shorter than the three P-O2 distances, 1.548 Å.

An alternative location of H2 is as an intra-PO_4 hydrogen bond of the type O1-H2···O2. Ferraris and Ivaldi (1984) have published a survey of such hydrogen bonds in protonated oxoanions including HPO_4. Extrapolating their results to the case of kintoreite, where P-O1 = 1.512 Å and O1-O2 = 2.52 Å, indicates that in this case the O1-H2 distance will be long, of the order of 1.3 Å. We were unable to directly confirm the existence of H2 from difference Fourier maps. This is not surprising, given that the proton will be offset from the threefold axis and the electron density corresponding to the single electron will thus be distributed over multiple partially occupied sites.

Zincian kintoreite. The refinement for zincian kintoreite reveals a structural feature that is new to the alunite-type minerals: the occupation of sites within the hexagonal rings of the octahedral layers. This is illustrated in Figure 4. The occupied sites are displaced from the centers of the rings by ~0.8 Å along directions <1$\bar{1}$0>, toward the six O3 anions (hydroxyl ions) forming the rings. Zn atoms partially occupy these sites, with a combined occupancy per hexagonal ring of 0.31(1). An atom located at the center of the hexagonal ring would have six equal distances of 2.70 Å to the O3 anions. The displacement of the Zn atom results in one short Zn-O3 distance of 1.91(1) Å and two longer Zn-O3 distances of 2.383(4) Å. Two short Zn-O1 distances of 1.72(1) and 1.86(1) Å, to the apical anions of the tetrahedra on either side of the ring, complete the trigonal bipyramidal coordination of Zn. The Zn atoms play a similar role to the hypothesized H2 protons in pure kintoreite, in helping to meet the bond valence requirements of the undersaturated O1 atoms. The trigonal bipyramidal coordination polyhedron for one of the Zn atoms and its linkages to the surrounding octahedra and tetrahedra are illustrated in Figure 5.

We have recently reported similar behavior of Zn occupying trigonal bipyramidal sites in a segnitite-type composition, $PbZn_{0.5}Fe_3(AsO_4)_2(OH)_6$ (Grey et al. 2008). The same type of coordination was obtained with three short and two longer distances. Such coordination occurs in other mineral structures containing HTB layers that have small cations occupying sites within the hexagonal rings. In zirconolite, Ti atoms are displaced from the centers of the rings and have 5-coordination with three short Ti-O distances of 1.83 to 1.89 Å and two longer distances at 2.23 Å (Gatehouse et al. 1981). The same type of coordination occurs for Ti in a pyrochlore phase with composition $(Ca_{0.75}Ti_{0.25})_2TiNbO_7$ (Roth et al. 2008). The pyrochlore structure has HTB-type octahedral layers perpendicular to the four equivalent <111> directions, and large cations such as Ca occupy the centers of the hexagonal rings and adopt 6+2 coordination. The replacement of a quarter of the Ca atoms by Ti in $(Ca_{0.75}Ti_{0.25})_2TiNbO_7$ is accompanied by a displacement of the Ti atoms by ~0.7 Å from the centers of the rings to take up trigonal bipyramidal coordination.

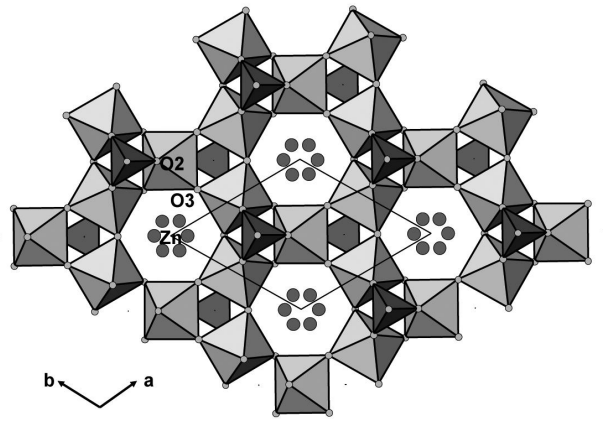

FIGURE 4. A (001) composite octahedral-tetrahedra layer in zincian kintoreite, showing displaced Zn atoms in the hexagonal rings as small filled circles.

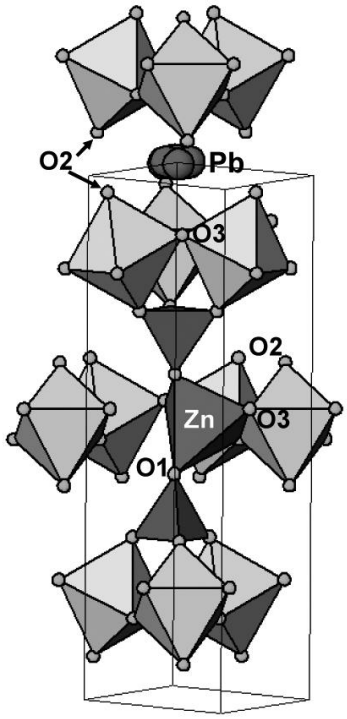

FIGURE 5. Stacking of polyhedra along [001] in zincian kintoreite, showing connectivity between the Zn-centered trigonal bipyramid and XO_4 tetrahedra. Two octahedra of the hexagonal ring surrounding the Zn atoms have been removed to show the Zn coordination.

In $PbZn_{0.5}Fe_3(AsO_4)_2(OH)_6$ (Grey et al. 2008), the Zn atoms are ordered into half of the available hexagonal rings, with a lowering of the symmetry from rhombohedral to monoclinic. Ordered displacements of the Pb atoms occur in response to the Zn ordering, with displacements of the Pb atoms away from the locations of the Zn atoms. In zincian kintoreite, there is only one Zn atom for every three hexagonal rings, but there is no indication of long-range ordering of Zn atoms and vacant sites as in $PbZn_{0.5}Fe_3(AsO_4)_2(OH)_6$. A good refinement of zincian kintoreite was obtained in $R\bar{3}m$, with a statistical distribution of Zn atoms in the sites in all hexagonal rings. The mixing of P and As at the X sites may play a role in preventing the development of long range order of the Zn atoms. The magnitude of the displacement of the Pb atom from the ideal site at (0,0,0) is 0.465 Å. This is considerably larger than the displacement of 0.394 Å for Pb in pure kintoreite. The larger displacement may be due to the larger volume of the zincian kintoreite cell (Table 2). However, it may also be in response to local ordering of Zn atoms, analogous to the long range ordering of Zn/Pb displacements in $PbZn_{0.5}Fe_3(AsO_4)_2(OH)_6$ (Grey et al. 2008).

Charge compensation in alunite-type minerals

The electron microprobe study of compositional variations in zincian kintoreite shows that the Zn has a strong negative correlation with S. Levels of Zn higher than 0.1 apfu occur only for compositions containing less than ~0.2 atoms of S pfu (≡0.9 wt% S). This observation, coupled with the published evidence for Zn substituting at the B site in high SO_4-containing compositions, suggests that the different modes of incorporation of Zn in Pb/(Fe,Al) alunite/jarosite-type minerals are in response to different charge balance requirements for compositions with $[SO_4]^{2-}$ dominant compared to compositions with $[(As,P)O_4]^{3-}$ dominant. The following charge balances apply: (1) $Pb(Fe,Al)_3(SO_4)_2(OH)_6$ → charge imbalance of +1; (2) $Pb(Fe,Al)_3(SO_4)(PO_4)(OH)_6$, and $Pb(Fe,Al)_3(SO_4)(AsO_4)(OH)_6$ → charge balanced; and (3) $PbFe_3(PO_4)_2(OH)_6$, and $PbFe_3(AsO_4)_2(OH)_6$ → charge imbalance of –1. Quite different charge balance mechanisms apply for the composition ranges 1 to 2 and 2 to 3. In the former case, the excess of positive charge is addressed in two main ways; by vacancies at the Pb site, as in plumbojarosite (Szymanski 1985), or by replacing trivalent Fe with a divalent ion (or vacancy) as in zincian beaverite, $PbFe_2(Cu,Zn)(SO_4)_2(OH)_6$ (Sato et al. 2008). Both cases occur in nature and depend on different conditions prevailing in solution at the time of crystallization, as demonstrated for synthetic plumbojarosite-beaverite solid solutions by Jambor and Dutrizac (1983).

In the composition range 2 to 3, the charge imbalance is of opposite sign and a different compensation mechanism is required. One possibility is protonation of the apical oxygen anions of the $(As,P)O_4$ tetrahedra, as discussed by Scott (1987) and Birch et al. (1992). This has been reported to be the mechanism for charge balance in gorceixite, $BaAl_3[(PO_4)(PO_3OH](OH)_6$ (Radoslovich 1982), and in crandallite, $CaAl_3[PO_3(O,OH)]_2(OH)_6$ (Blount 1974). An alternative compensation mechanism, as found for zincian kintoreite, involves the location of a divalent ion halfway between the apical anions of pairs of $(P,As)O_4$ tetrahedra (Fig. 5). The Zn atoms are displaced within the hexagonal rings of the octahedral layers such that they help meet the valence requirements of the tetrahedral apical anions while also meeting their own bonding and valence requirements. Other ions with a similar ionic radius for five-coordination, such as Cu^{2+}, Fe^{2+}, and Li^{+}, may also occupy the new site. Incorporation of elements like Zn^{2+} into the hexagonal rings of P/As-rich alunite-type minerals will occur when the crystallization conditions (pH, ions in solution, etc.) are energetically more favorable for such an incorporation than for protonation of the apical anions of the $(P,As)O_4$ tetrahedra. It is possible that both charge-compensating mechanisms can coexist under certain conditions.

Although this new charge compensation mechanism has not been previously reported, apart from our recent study on monoclinic $PbZn_{0.5}Fe_3(AsO_4)_2(OH)_6$ (Grey et al. 2008), it may be quite common for $A^{2+}B_3^{3+}(XO_4)_2(OH)_6$ minerals with low S contents. A clue to its possible presence can be found from an inspection of published analyses for such minerals. Analyses that give formulae containing an excess of B cations (>3 pfu) could warrant structural studies to check for the presence of cations within the hexagonal rings of the HTB layers. A search of the literature reveals several crandallite-group minerals as potential candidates. Analyses of crandallite, $CaAl_3[PO_3(O,OH)]_2(OH)_6$, minerals containing variable Sr, REE, and Th from a bauxite deposit in Timan, Russia (Mordberg et al. 2001), and from the Mt. Weld carbonatite laterite, Western Australia (Lottermoser 1990), consistently show the sum of X atoms to be <2 and the sum of the B atoms to be >3. In the former case, the average of 27 microprobe analyses, normalized to 14 anions, gives the cation ratio $A:B_{3.4}:X_{1.9}$.

More extreme examples of this type are triclinic crandallite from clay sediments in Guatemala (Cowgill et al. 1963), and eylettersite, with dominant Th in the A site (van Wambeke 1972), where the deficiency in PO_4 is of the order of 0.5 moles pfu and the excess of Al is 0.5 apfu. The P deficiency has been explained (van Wambeke 1971) as being due to replacement of PO_4 by the tetrahydroxy group H_4O_4, analogous to H_4O_4 replacing SiO_4 in hydrogarnets. McConnell (1965) has proposed this model to explain P deficiency in apatite.

A possible explanation for the excess Al in these minerals is that it occupies sites within the hexagonal rings of the octahedral layers, similar to those occupied by Zn in kintoreite, and provides charge balance for the excess of negative charge brought about by the substitution of $(H_4O_4)^{4-}$ for $(PO_4)^{3-}$. An ideal formula for triclinic crandallite is $Ca(Al_{0.5})Al_3[(PO_4)_{1.5}(H_4O_4)_{0.5}](OH)_6$, where $(Al_{0.5})$ occupies displaced sites in the hexagonal rings of the octahedral layers. We have recently shown from a single-crystal refinement of Al-containing zirconolite, that the Al atoms occupy such sites (Grey et al. 2003). In contrast to Zn in kintoreite, which is displaced toward one of the anions forming the hexagonal ring, to establish trigonal bipyramidal coordination, Al in zirconolite is displaced toward an O-O edge of the ring, to assume tetrahedral coordination.

In his review of the nomenclature of the alunite supergroup, Jambor (1999) concluded that eylettersite and the possible triclinic analog of crandallite both require re-examination because of the deviation of their compositions from the generic formula. We support his suggestion, particularly as a structural study of these samples will clarify whether they fit into the same category as monoclinic $PbZn_{0.5}Fe_3(AsO_4)_2(OH)_6$ and zincian kintoreite.

ACKNOWLEGMENTS

We thank C. Forsyth for collecting the single-crystal data. Thanks to reviewers for helpful comments.

REFERENCES CITED

Baur, W.H. (1981) Interatomic distance predictions for computer simulation of crystal structures. In M. O'Keeffe and A. Navrotsky, Eds., Structure and Bonding in Crystals II, p. 31–52. Academic Press, New York.

Birch, W.D. and van der Heyden, A. (1997) Minerals from the Kintore and Block 14 open cuts at Broken Hill, New South Wales. Australian Journal of Mineralogy, 3, 23–71.

Birch, W.D., Pring, A., and Gatehouse, B.M. (1992) Segnitite, $PbFe_3H(AsO_4)_2(OH)_6$, a new mineral in the lusingite group, from Broken Hill, New South Wales. American Mineralogist, 77, 656–659.

Blount, A.M. (1974) The crystal structure of crandallite. American Mineralogist, 59, 41–47.

Brese, N.E. and O'Keeffe, M. (1991) Bond-valence parameters for solids. Acta Crystallographica, B47, 192–197.

Cowgill, U.M., Hutchinson, G.E., and Joensuu, O. (1963) An apparently triclinic dimorph of crandallite from a tropical swamp sediment in El Peten, Guatemala. American Mineralogist, 48, 1144–1153.

Dzikowski, T.J., Groat, L.A., and Jambor, J.L. (2006) The symmetry and crystal structure of gorceixite, $BaAl_3[PO_3(O,OH)]_2(OH)_6$, a member of the alunite supergroup. Canadian Mineralogist, 44, 951–958.

Farrugia, L.J. (1999) WinGX suite for small-molecule single-crystal crystallography. Journal of Applied Crystallography, 32, 837–838.

Ferraris, G. and Ivaldi, G. (1984) *X*-OH and O-H···O bond lengths in protonated oxoanions. Acta Crystallographica, B40, 1–6.

Gatehouse, B.M., Grey, I.E., Hill, R.J., and Rossell, H.J. (1981) Zirconolite, $CaZr_xTi_{3-x}O_7$; structure refinements for near-end-member compositions with x = 0.85 and 1.30. Acta Crystallographica, B37, 306–312.

Giuseppetti, G. and Tadini, C. (1980) The crystal structure of osarizawaite. Neues Jahrbuch für Mineralogie, Monatshefte, 401–407.

——— (1987) Corkite $PbFe_3(SO_4)(PO_4)(OH)_6$, its crystal structure and ordered arrangement of tetrahedral cations. Neues Jahrbuch für Mineralogie, Monatshefte, 71–81.

——— (1989) Beudantite: $PbFe_3(SO_4(AsO_4)(OH)_6$, its crystal structure, tetrahedral site disordering and scattered Pb distribution, Neues Jahrbuch für Mineralogie, Monatshefte, 27–33.

Gottlicher, J. and Gasharova, B. (1999) Can jarosite be monoclinic? European Journal of Mineralogy, 11, 86.

Grey, I.E., Mumme, W.G., Ness, T.J., Roth, R.S., and Smith, K.L. (2003) Structural relations between weberite and zirconolite polytypes-refinements of doped 3T and 4M $Ca_2Ta_2O_7$ and 3T $CaZrTi_2O_7$. Journal of Solid State Chemistry, 174, 285–295.

Grey, I.E., Birch, W.D., Bougerol, C., and Mills, S.J. (2006) Unit-cell intergrowth of pyrochlore and hexagonal tungsten bronze structures in secondary tungsten minerals. Journal of Solid State Chemistry, 179, 3834–3843.

Grey, I.E., Mumme, W.G., Bordet, P., and Mills, S.J. (2008) A new crystal-chemical variation of the alunite-type structure in monoclinic $PbZn_{0.5}Fe_3(AsO_4)_2(OH)_6$. Canadian Mineralogist, 46, 1355–1364.

Jambor, J.L. (1999) Nomenclature of the alunite supergroup. Canadian Mineralogist, 37, 1323–1341.

Jambor, J.L. and Dutrizac, J.E. (1983) Beaverite-plumbojarosite solid solutions. Canadian Mineralogist, 21, 101–113.

Kharisun, Taylor, M.R., Bevan, D.J.M., and Pring, A. (1997) The crystal structure of kintoreite, $PbFe_3(PO_4)_2(OH,H_2O)_6$. Mineralogical Magazine, 61, 123–129.

Kolitsch, U. and Pring, A. (2001) Crystal chemistry of the crandallite, beudantite, and alunite groups: A review and evaluation of the suitability as storage materials for toxic metals. Journal of Mineralogical and Petrological Sciences, 96, 67–78.

Kolitsch, U., Tiekink, E.R.T., Slade, P.G., Taylor, M.R., and Pring, A. (1999) Hinsdalite and plumbogummite, their atomic arrangements, and disordered lead sites. European Journal of Mineralogy, 11, 513–520.

Lottermoser, B.G. (1990) Rare earth element mineralisation within the Mt. Weld carbonatite laterite, Western Australia. Lithos, 24, 151–167.

McConnell, D. (1965) Deficiency of phosphate ions in apatite. Naturwissenschaften, 52, 183.

Mills, S.J., Kolitsch, U., and Birch, W.D. (2006) Crystal-chemical behaviour of Ge and Ga in Pb–Fe members of the alunite supergroup. 19th General Meeting of the International Mineralogical Association (IMA), Kobe, Japan.

Mordberg, L.E., Stanley, C.J., and Gerkmann, K. (2001) Mineralogy and geochemistry of trace elements in bauxites: the Devonian Schugorsk deposit, Russia. Mineralogical Magazine, 65, 81–101.

Nakamoto, K., Margoshes, M., and Rundle, R.E. (1955) Stretching frequencies as a function of distances in hydrogen bonds. Journal of the American Chemical Society, 77, 6480–6486.

Petricek, V. and Dusek, M. (2000) JANA2000, a Crystallographic Computing System. Institute of Physics, Academy of Sciences of the Czech Republic, Prague.

Pouchou, J.L. and Pichoir, F. (1993) Films and stratified specimens. Scanning Electron Microscopy Supplement, 7, 167–189.

Radoslovich, E.W. (1982) Refinement of the gorceixite structure in Cm. Neues Jahrbuch für Mineralogie, Monatshefte, 446–464.

Rattray, K.J., Taylor, M.R., Bevan, D.J.M., and Pring, A. (1996) Compositional segregation and solid solution in the lead-dominant alunite-type minerals from Broken Hill, N.S.W. Mineralogical Magazine, 60, 779–785.

Roth, R.S., Vanderah, T.A., Bordet, P., Grey, I.E., Mumme, W.G., Cai, L., and Nino, J.C. (2008) Pyrochlore formation, phase relations, and properties in the CaO-TiO_2-$(Nb,Ta)_2O_5$ systems. Journal of Solid State Chemistry, 181, 406–414.

Sato, E., Nakai, I., Terada, Y., Tstusumi, Y., Yokoyama, K., Miyawaki, R., and Mastubara, S. (2008) Study of Zn-bearing beaverite $Pb(Fe_2Zn)(SO_4)_2(OH)_6$ obtained from Mikawa mine, Niigata Prefecture, Japan. Journal of Mineralogical and Petrological Sciences, 103, 141–144.

Scott, K.M. (1987) Solid solution in, and classification of, gossan-derived members of the alunite-jarosite family, northwest Queensland, Australia. American Mineralogist, 72, 178–187.

Sheldrick, G.M. (1997) SHELXL-97, A program for crystal structure refinement. University of Göttingen, Germany.

Szymanski, J.T. (1985) The crystal structure of plumbojarosite $Pb[Fe_3(SO_4)_2(OH)_6]_2$. Canadian Mineralogist, 23, 659–668.

——— (1988) The crystal structure of beudantite, $Pb(FeAl)_3[(As,S)O_4]_2(OH)_6$. Canadian Mineralogist, 26, 923–932.

van Wambeke, L. (1971) The problem of cation deficiencies in some phosphates due to alteration processes. American Mineralogist, 56, 1366–1384.

——— (1972) Eylettersite, un nouveau phosphate de thorium appartenant a la serie de la crandallite. Bulletin Societe Francaise, Mineralogie et Cristallographie, 95, 98–105.

MANUSCRIPT RECEIVED SEPTEMBER 1, 2008
MANUSCRIPT ACCEPTED DECEMBER 29, 2008
MANUSCRIPT HANDLED BY HONGWU XU